Dynamical Excimer Formation in Rigid Carbazolophane via Charge Transfer State

Tamai, Yasunari; Ohkita, Hideo; Shimada, Jiro; Benten, Hiroaki; Ito, Shinzaburo; Yamanaka, Sho; Hisada, Kenji; Tani, Keita; Kubono, Koji; Shinmyozu, Teruo

CITATION:

Tamai, Yasunari ...[et al]. Dynamical Excimer Formation in Rigid Carbazolophane via Charge Transfer State. The Journal of Physical Chemistry A 2013, 117(33): 7776-7785

ISSUE DATE:

2013-08-22

URL:

http://hdl.handle.net/2433/279591

Dynamical Excimer Formation in Rigid Carbazolophane via Charge Transfer State

Yasunari Tamai,[†] Hideo Ohkita,[,†] Jiro Shimada,[†] Hiroaki Benten,[†] Shinzaburo Ito,[†] Sho Yamanaka,[‡] Kenji Hisada,[‡] Keita Tani,[††] Koji Kubono,[††] and Teruo Shinmyozu[‡‡]*

[†]Department of Polymer Chemistry, Graduate School of Engineering, Kyoto University, Katsura, Nishikyo-ku, Kyoto 615-8510, Japan

[‡]Department of Frontier Fiber Technology and Science, Graduate School of Engineering, University of Fukui, 3-9-1 Bunkyo, Fukui 910-8507, Japan

[††]Division of Natural Science, Osaka Kyoiku University, Asahigaoka, Kashiwara, Osaka 582-8582, Japan

[‡‡]Institute for Materials Chemistry and Engineering, Kyushu University, Hakozaki, Higashi-ku, Fukuoka 812-8581, Japan

E-mail: ohkita@photo.polym.kyoto-u.ac.jp

RECEIVED DATE (to be automatically inserted after your manuscript is accepted if required according to the journal that you are submitting your paper to)

CORRESPONDING AUTHOR FOOTNOTE.

[†]Kyoto University.

[‡]University of Fukui.

[††]Osaka Kyoiku University.

[‡‡]Kyushu University.

TITLE RUNNING HEAD: Excimer Formation in Carbazolophane

Abstract

Formation dynamics of intramolecular excimer in dioxa[3.3](3,6)carbazolophane (CzOCz) was studied by time-resolved spectroscopic methods and computational calculations. In the ground state, the most stable conformer in CzOCz is the *anti*-conformation where two carbazole rings are aligned in anti-parallel. No other isomers were observed even after the solution was heated up to 150 °C, although three characteristic isomers are found by the molecular mechanics calculation: the first is the *anti*-conformer, the second is the *syn*-conformer where two carbazole rings are stacked in the same direction, and the third is the *int*-conformer where two carbazole rings are aligned in an edge-to-face geometry. Because of the *anti*-conformation, the interchromophoric interaction in CzOCz is negligible in the ground state. Nonetheless, the intramolecular excimer in CzOCz was dynamically formed in an acetonitrile (MeCN) solution, indicating strong interchromophoric interaction and the isomerization from the *anti*- to *syn*-conformation in the excited state. The excimer formation in CzOCz is more efficient in polar solvents than in less polar solvents, suggesting the contribution of the charge transfer (CT) state to the excimer formation. The stabilization in the excited state is discussed in terms of molecular orbital interaction between two carbazole rings. The solvent-polarity-induced excimer formation is discussed in terms of the CT character in the *int*-conformation.

KEYWORDS (Word Style “BG_Keywords”). carbazole, cyclophane, intramolecular excimer, time-dependent DFT, edge-to-face geometry

BRIEFS (WORD Style “BH_Briefs”). If you are submitting your paper to a journal that requires a brief, provide a one-sentence synopsis for inclusion in the Table of Contents.

1. Introduction

Intramolecular excimer has attracted much attention from the view point of the relationship between the molecular structure and the formation dynamics.[1–8] The intramolecular excimers can be formed when the stabilization energy due to exciton and charge resonance interactions exceeds the conformational instability.[9–14] Previous studies have shown that the intramolecular singlet excimer is the most stable when the two chromophores can overlap in a symmetric sandwich or totally eclipsed geometry. On the other hand, Lim et al. proposed the L-shaped structure of the triplet excimers of naphthalene, which is stabilized mostly by charge transfer (CT) interaction.[15–17] In other words, the intramolecular excimer formation is strongly dependent on conformational rearrangement in the excited state. Solvent-polarity-induced intramolecular excimer was first observed for 1,2-di(1-anthryl)ethane where the excimer formation was promoted in polar solvents.[18–20] The solvent-polarity dependence is a clear indication of an intermediate CT state in the excimer formation process. Their result suggests that the activation energy of the conformational rearrangement is reduced in the CT state, and hence the excimer is formed more easily.

Cyclophanes are one of the most reliable molecules for studying the intermolecular interactions between two chromophoric groups not only in the ground state but also in the excited state,[21–25] because they have a rigid structure where the relative geometry of two chromophoric groups is clearly defined. In particular, various *syn*-cyclophanes have been studied to examine excimer properties in terms of their structures.[26–36] On the other hand, the *anti*-cyclophanes have a structure where two chromophores are bridged in anti-parallel geometry. Thus, the *anti*–*syn* isomerization in the *anti*-cyclophanes is difficult in the ground state because of large activation energy.[37–45] Nonetheless, the intramolecular excimer formation in the *anti*-cyclophanes has been reported by several groups.[39–41] Mataga et al. reported the intramolecular excimer formation in metapyrenophane (mePy).[40,41] Interestingly, the intramolecular excimer in mePy is formed only in polar solvents. They speculated that conformational change in mePy would be favorable in the CT state similarly to the case of 1,2-di(1-anthryl)ethane.[41] However, the direct observation of intramolecular excimer formation dynamics in rigid *anti*-cyclophanes has not been

reported so far and the relationship between the CT state and the excimer formation dynamics is not fully understood.

Herein, we study the intramolecular excimer formation dynamics in a carbazolophane, dioxa[3.3](3,6)carbazolophane (CzOCz, the chemical structure is shown in Figure 1) in which two *N*-ethylcarbazole rings are linked at 3 and 6 positions with CH_2OCH_2 bridges.[45] Previously, we showed that the stacking mode of two carbazole rings in CzOCz is the *anti*-conformation in the ground state as shown in Figure 1, and hence no excimer emission is observed for CzOCz in a 2-methyltetrahydrofuran solution. In this study, we found that CzOCz exhibits a clear excimer emission in polar solvents such as acetonitrile (MeCN). This result suggests that the conformational rearrangement in CzOCz would be promoted in the CT state. In terms of the conformation of CzOCz, we discuss the solvent-polarity-induced intramolecular excimer formation dynamics experimentally by using time-resolved spectroscopic methods and computationally by using molecular mechanics and density functional theory (DFT).

2. Results

2.1. ^{1}H NMR of CzOCz in Solution. As shown in Figure 1, there are at least two possible isomers in CzOCz: one is *syn*-conformer (*syn*-CzOCz) where two carbazole rings are fully overlapped, and the other is *anti*-conformer (*anti*-CzOCz) where two carbazole rings are aligned in anti-parallel geometry. To identify the isomeric structure in the ground state, we measured ^{1}H NMR spectra of CzOCz and CzOMe (a reference monomer) in a DMSO-d_6 solution at room temperature. As summarized in Table 1, the chemical shifts of the aromatic protons in CzOCz are almost the same as those of CzOMe. The difference between them is as small as <0.1 ppm, indicating that two carbazole rings in CzOCz are far apart and little overlapped in the *anti*-conformation as reported previously.[45] No distinct difference in the chemical shift was observed even at 150 °C, suggesting that the isomerization from *anti*- to *syn*-conformation is negligible in the ground state because of large activation energy.

-----<<< Figure 1 >>>-----

-----<<< Table 1 >>>-----

2.2. Absorption and Fluorescence Spectra. Figure 2a shows the absorption spectra of CzOCz and CzOMe in an MeCN solution at room temperature. There is no distinct difference in the absorption spectra between CzOCz and CzOMe, which is consistent with the *anti*-conformation of CzOCz in the ground state. The absorption bands at 300 and 350 nm are assigned to the $^1L_a \leftarrow {}^1A$ and $^1L_b \leftarrow {}^1A$ transitions, respectively.[46–48] On the other hand, as shown in Figure 2b, there is a clear difference in the fluorescence spectra between CzOCz and CzOMe in an MeCN solution at room temperature. In the fluorescence spectrum of CzOCz (black solid), a strong vibronic emission band was observed at around 360 nm and a weak and broad emission band was additionally observed at around 430 nm. The emission band at 360 nm is in good agreement with that of CzOMe and hence is ascribed to the monomer emission band. The structureless shoulder peak around 430 nm disappeared after O_2 bubbling (black broken), suggesting that this band is due to a long-lived excited species. As shown by the red line in the figure, the differential spectrum before and after O_2 bubbling exhibits a broad emission band without vibrational structures, which is in good agreement with the carbazole excimer emission reported previously.[30–36,47] Note that no excimer emission was observed for the CzOMe solution under the same concentration. Thus, the broad emission at 430 nm is ascribed to the intramolecular excimer of CzOCz in MeCN. In summary, the interchromophoric interaction in CzOCz is negligible in the ground state but considerable in the excited state.

-----<<< Figure 2 >>>-----

Figure 2c shows the fluorescence spectra of CzOCz in different solutions: MeCN (dielectric constant ε_r = 37.5, solvent viscosity η = 0.35 cP), *N*,*N*-dimethyl formamide (DMF; ε_r = 36.7, η = 0.92 cP), and tetrahydrofuran (THF; ε_r = 7.58, η = 0.55 cP). The excimer emission intensity was much stronger in a

more polar MeCN than in a less polar THF solution, suggesting that the excimer formation is more efficient in polar solvents with higher dielectric constants. It is noteworthy that the peak wavelength of the excimer band was independent of the dielectric constant of solvents as described below. On the other hand, the excimer emission intensity was much stronger in the less viscous MeCN than in the more viscous DMF solution, indicating that the excimer formation is accompanied by some conformational rearrangements, most probably *anti–syn* isomerization in the excited state as will be discussed later. In summary, the excimer formation in CzOCz is favorable in solvents with a higher dielectric constant and lower viscosity.

2.3. Time-Resolved Emission. To examine the excimer formation dynamics, we measured the time-resolved emission spectra and decay of CzOCz in MeCN, DMF, and THF solutions. As shown in Figure 3a, a sharp monomer band was observed at 360 nm immediately after the laser excitation and then decayed in a few nanoseconds. Subsequently, a broad excimer band was observed at 430 nm after several ten nanoseconds. This temporal change in the emission spectra clearly shows the dynamical formation of the intramolecular excimer from the monomer state. The peak wavelength of the excimer band was neither shifted with time nor dependent on the solvent polarity. Figure 3b shows the time evolution of the monomer band at 360 nm (triangles and squares) and the excimer band at 450 nm (circles). The decay of the monomer band was fitted by a single exponential function, and the rise and decay of the excimer band was fitted by double exponential functions. As summarized in Table 2, the decay constant of the monomer band (τ_{mono}) is shorter than that of the reference emission of CzOMe (τ_f^0) and is in good agreement with the rise constant of the excimer band. The coincidence in the rise and decay constants is kinetic evidence for the dynamical formation of the intramolecular excimer in CzOCz. The apparent excimer formation rate constant $k_{ex} = 1/\tau_{mono} - 1/\tau_f^0$ was estimated to be 5.6×10^8 s^{-1} in an MeCN solution, 2.1×10^8 s^{-1} in a DMF solution, and 1.3×10^8 s^{-1} in a THF solution. This trend in k_{ex} is consistent with that in the excimer intensity as mentioned above, and thus again indicates that the excimer formation in CzOCz is accompanied by some conformational rearrangements in the excited

state and is more rapid in polar solvents. As listed in Table 2, the decay constant of the excimer emission was longer than that of CzOMe monomer emission, indicating that the excimer emission is symmetrically forbidden as reported previously,[33–35,47] and hence the CzOCz excimer is *syn*-conformation rather than *anti*-conformation. Furthermore, the decay constant was independent of solvents, suggesting that the excimer conformation is independent of solvent polarity and viscosity and that CT character of the excimer state is negligibly small.

-----<<< Figure 3 >>>-----

-----<<< Table 2 >>>-----

Figure 4 shows the Arrhenius plots of k_{ex} of CzOCz in an MeCN solution against the temperature ranging from 273 to 323 K. The solid line represents a fitting curve by the Arrhenius equation: $k_{ex} = A \exp(-E_a/RT)$ where A is the pre-exponential factor and E_a is the apparent activation energy for the excimer formation. The pre-exponential factor A was estimated to be 8.6×10^{10} s^{-1} for all the solvents employed. Thus, the difference in the excimer formation efficiency is attributed to the activation energy difference. The apparent activation energy E_a was estimated to be 12.3 kJ mol^{-1} in an MeCN solution and 16.1 kJ mol^{-1} in a THF solution. Because the activation energy due to solvent viscosity E_η has been reported to be about 7.1 kJ mol^{-1} (MeCN) and 7.5 kJ mol^{-1} (THF),[49,50] the activation energy for the isomerization E_{iso} was estimated to be as low as 5.2 kJ mol^{-1} (MeCN) and 8.6 kJ mol^{-1} (THF). This finding indicates that the potential barrier for the isomerization is much lower than that in the ground state and becomes lower in polar solutions as will be discussed later.

-----<<< Figure 4 >>>-----

2.4. Transient Absorption. Figure 5 shows the transient absorption spectra of CzOCz and CzOMe in various solutions measured from 1 ps to 3 ns after the laser excitation at 350 nm. Immediately after the

laser excitation at 1 ps, two absorption bands were observed at 650 and 1100 nm for all the solutions. These bands are ascribed to the $S_n \leftarrow S_1$ absorption of the carbazole monomer as reported previously.[35,51] In other words, the primary photoexcitation in CzOCz is localized onto one carbazole ring because CzOCz is *anti*-conformation in the ground state. On a time scale of nanoseconds, a new absorption band gradually increased at around 900 nm. The rise time of this band was estimated to be 1.2 ns for CzOCz in an MeCN solution, which is in good agreement with the excimer rise time mentioned above (data is shown in the Supporting Information). At 3 ns after the laser excitation (red solid), the new band was observed for all three solutions. As reported previously, this band is ascribed to the charge transfer (CT) band of carbazole excimer as shown in Scheme 1 and the spectral position of the band is sensitive to the relative geometry of two carbazole rings.[35] As shown in Figure 5, the peak wavelength was independent of the solvent employed, which is consistent with the time-resolved emission spectra. Thus, these findings suggest that the conformation of CzOCz excimer is almost the same for all the solvents employed. Note that no remarkable absorption change was observed for the band at 650 nm. This is because the $S_n \leftarrow S_1$ absorption of the carbazole monomer is almost the same as the local excitation (LE) band of the carbazole excimer (Scheme 1).[35] It is also noted that other transients such as radical ion or ion pair were not observed under this experimental conditions.

-----<<< Figure 5 >>>-----

-----<<< Scheme 1 >>>-----

2.5. Molecular Mechanics and Quantum Chemical Calculations. To find the most stable conformation, we calculated the potential energy surface of CzOCz in the ground state by using the AMBER force field[52] where the dihedral angles φ_1 and φ_2 are defined as shown in Figure 6a. As a result, three local potential minima were found as shown in Figure 6b. The first one is the *anti*-conformer with $\varphi_1 \approx \varphi_2 \approx -50$ ° where two carbazole rings are aligned in anti-parallel. The second one is the *syn*-

conformer with $\varphi_1 \approx -75$ ° and $\varphi_2 \approx 75$ ° where two carbazole rings are aligned in parallel. The third one is an intermediate conformer with $\varphi_1 \approx -150$ ° and $\varphi_2 \approx 70$ ° where two carbazole rings are rather stacked in an edge-to-face geometry (hereafter abbreviated as *int*-conformation). As shown in Figure 6b, the *anti–syn* isomerization via the *int*-conformer is the most probable although it is still thermodynamically unfavorable because of the high potential barrier (60 kJ mol^{-1}) in the ground state. This is consistent with our observation that only *anti*-CzOCz exists in the ground state as mentioned above. As shown in Figure 6c, the potential barrier is higher in the *anti–int* isomerization than in the *int–syn* isomerization, suggesting that the *anti–int* isomerization is more difficult than the *int–syn* isomerization. This is probably true in the excited state although the potential is calculated in the ground state. Thus, the *anti–int* isomerization would be more difficult than the *int–syn* isomerization in the excited state as will be discussed later. Here we consider symmetric isomerization pathway alone in the AMBER calculations: the dihedral angles in the opposite side, φ_1' and φ_2', are assumed to be equal to φ_1 and φ_2, respectively. Full detail of the isomerization is described in the Supporting Information. We note that basically the same three conformers are obtained even though asymmetric isomerization pathways are considered.

-----<<< Figure 6 >>>-----

Next, we calculated the optimized structures of these three stable CzOCz conformers in the ground (excited) states by (time-dependent) density functional theory ((TD-)DFT) at the (TD-)DFT/CAM-B3LYP level with the 6-31G(d,p) basis set.[53,54] In the ground state, *anti*-CzOCz is the most stable and *int*-CzOCz is the most unstable among three conformers, both of which are consistent with the AMBER calculations. For *anti*-CzOCz and *int*-CzOCz, as shown in Figure 7a, no distinct difference in the conformation is observed between the ground and excited state. For *syn*-CzOCz, the interchromophoric distance is shorter in the excited state than in the ground state, resulting from the attractive interchromophoric interaction in the excited state. Figure 7b shows the relevant molecular orbitals of

these three CzOCz conformers in the excited state conformation. In the *anti*-CzOCz, small orbital overlap is in good agreement with localization of the primary photoexcitation onto one carbazole ring as mentioned above. In the *syn*-CzOCz, the LUMO is symmetrically delocalized over two carbazole chromophores in contrast to the *anti*-CzOCz, suggesting considerable interchromophoric interaction. Interestingly, the molecular orbitals in the *int*-CzOCz are distributed asymmetrically between two carbazole chromophores: the HOMO and LUMO+1 are almost localized onto one carbazole ring and the HOMO−1 and LUMO are almost localized onto another ring as will be discussed later.

To discuss the CT character of the CzOCz conformers in the excited states, we analyzed the change in the Mulliken charge upon excitation as shown in Figure 8. For *anti*- and *syn*-CzOCz, no difference in the Mulliken charge was observed for two carbazole rings, suggesting no CT character in the excited state. This is consistent with the solvent-polarity independent emission observed for the *anti*-CzOCz and *syn*-CzOCz as mentioned above. For *int*-CzOCz, on the other hand, asymmetric distribution of the Mulliken charge was observed: the upper (axial) carbazole ring was negatively charged while the lower (facial) ring was positively charged in the edge-to-face geometry as shown in Figure 8b. This finding indicates a CT character of *int*-CzOCz in the excited state as will be discussed later.

To compare the relative stability in these three CzOCz conformers, we calculated the energy difference between the optimized conformers in the excited state ΔE. In contrast to the ground state, the *anti*-conformer is the most unstable in the excited state, suggesting the attractive interaction between two carbazole rings in the *int*- and *syn*-conformations in the excited state. As summarized in Table 3, the energy difference between the *anti*- and *int*-conformers ΔE_{ai} increases from −1.8 to −8.8 kJ mol^{-1} with increasing surrounding polarity. On the other hand, the energy difference between the *anti*- and *syn*-conformations ΔE_{as} remains the same at ~ −15 kJ mol^{-1} independently of the surrounding polarity. This polarity dependence indicates that the *int*-CzOCz has a CT character in the excited state while the *syn*-CzOCz in the excited state is rather neutral as mentioned above. It is noteworthy that the vertical excitation energy from the ground to the excited state E_{vert} for *anti*- and *syn*-conformers is independent of the surrounding polarity, which is consistent with the polarity-independent emission mentioned above.

-----<<< Figures 7,8 >>>-----

-----<<< Table 3 >>>-----

3. Discussion

3.1. Kinetics of the Intramolecular Excimer Formation. In order to analyze the formation dynamics of intramolecular excimer in CzOCz, we propose the kinetic scheme as shown in Scheme 2. Thus, the rate equations are described by Eq. 1

$$\begin{aligned} \frac{\mathrm{d}A(t)}{\mathrm{d}t} &= -k_{\mathrm{d}1}A(t) - k_{ai}A(t) + k_{ia}I(t) \\ \frac{\mathrm{d}I(t)}{\mathrm{d}t} &= -k_{\mathrm{d}2}I(t) + k_{ai}A(t) - k_{ia}I(t) - k_{is}I(t) + k_{si}S(t) \\ \frac{\mathrm{d}S(t)}{\mathrm{d}t} &= -k_{\mathrm{d}3}S(t) + k_{is}I(t) - k_{si}S(t) \end{aligned} \qquad (1)$$

where $A(t)$, $I(t)$, and $S(t)$ are the density of the *anti*-, *int*-, and *syn*-CzOCz in the excited state at a delay time t after the laser excitation, $k_{\mathrm{d}1}$, $k_{\mathrm{d}2}$, and $k_{\mathrm{d}3}$ are the rate constants of the radiative and non-radiative deactivations in the *anti*-, *int*-, and *syn*-CzOCz, respectively, and k_{ai}, k_{is}, k_{ia}, and k_{si} are the isomerization rate constants in the excited state. On the basis of the energy difference calculated above, it can be safely said that $k_{ai} >> k_{ia}$ and $k_{is} >> k_{si}$, which is consistent with the single exponential decay of the monomer emission in CzOCz. Furthermore, it can be set that $k_{ai} << k_{is}$ because $I(t) \approx 0$: no observation of the *int*-CzOCz in the time-resolved fluorescence and transient absorption measurements. In other words, the *anti*–*int* isomerization is the rate-limiting process for the excimer formation in CzOCz (see the Supporting Information). Under these conditions, $A(t)$ and $S(t)$ are simply described by Eq. 2 (details are described in the Supporting Information).

$$\begin{aligned} A(t) &= A_0\exp[-(k_{\mathrm{d}1}+k_{ai})t] \\ S(t) &= \frac{k_{ai}}{k_{\mathrm{d}1} + k_{ai} - k_{\mathrm{d}3}}A_0\{\exp(-k_{\mathrm{d}3}t) - \exp[-(k_{\mathrm{d}1}+k_{ai})t]\} \end{aligned} \qquad (2)$$

Therefore, the apparent excimer formation rate constant can be considered to be the same as $k_{ai} = 1/\tau_{mono} - k_{d1}$. Assuming that k_{d1} is the same as the decay rate constant of the CzOMe, k_{ai} is described as $k_{ai} \approx 1/\tau_{mono} - 1/\tau_f^0 = k_{ex}$ where τ_f^0 is the fluorescence lifetime of the CzOMe. Thus, the k_{ex} and E_{iso} evaluated above corresponds to the rate constant and the activation energy for the *anti–int* isomerization, respectively. We therefore conclude that the efficient excimer formation in polar solutions is attributed to the reduction in the potential barrier for the *anti–int* isomerization of CzOCz in the excited state.

-----<<< Scheme 2 >>>-----

3.2. Excimer Formation Mechanism. On the basis of the kinetic analysis described above, the intramolecular excimer formation in CzOCz can be summarized as shown in Scheme 3. In the ground state, the *anti*-conformation is more stable than the *int*- and *syn*-conformations. This is because both bonding and anti-bonding orbitals are filled with electrons in the ground state and hence favorable and unfavorable orbital interaction is canceled out in the dimer geometry. Rather, the repulsive interchromophoric interaction increases as two carbazole rings are approaching in the ground state. As a result, the *anti*-conformation is the most stable because of the smallest ring overlap. As shown in Scheme 3, the potential barrier from the *anti*- to *int*-CzOCz is so high that the *anti–int* isomerization is negligible (arrow a): only *anti*-CzOCz exists in the ground state. In contrast, the *anti*-conformation is the most unstable in the excited state as summarized in Table 3, suggesting that the attractive interaction between two carbazole rings in the *int*- and *syn*-conformations is considerably large in the excited state. In the dimer geometry, the LUMO is a bonding orbital and the HOMO is an anti-bonding orbital. Thus, the favorable interaction is enhanced by the electron transition from HOMO to LUMO. On the other hand, the stabilization energy is dependent on the interchromophoric interaction in CzOCz, which is most sensitive to the interchromophoric distance. Thus, *syn*-CzOCz is the most stable and *anti*-CzOCz is the most unstable in the excited state.[9–14,55] The stabilization of *int*-CzOCz in the excited state leads to the decrease in the potential barrier, resulting in the efficient *anti–int* isomerization (arrow b). Once

anti-CzOCz converts to *int*-CzOCz, it immediately further converts to *syn*-CzOCz, because the *int–syn* isomerization rate is much larger than the *anti–int* isomerization rate as mentioned above (arrow c). The *int*-CzOCz in polar solutions is more stable because of the CT character in the excited state, resulting in the lower potential barrier for the *anti–int* isomerization. Thus, the *anti–int* isomerization is more efficient in polar solutions. We therefore conclude that the CT character of the *int*-CzOCz in the excited state is a key determinant for the solvent-polarity-induced intramolecular excimer formation.

-----<<< Scheme 3 >>>-----

3.3. Origin of the CT Character of *int*-CzOCz. We finally discuss the origin of the CT character even in a homodimer with two carbazole groups. Intramolecular CT in the dimer of identical chromophores was first reported for 1,2-di(1-anthryl)ethane in polar solutions by Mataga et al.[18,19,56–59] They found that anthracene radical cation and anion are formed first because of strong intramolecular CT character and then intramolecular excimer is formed by recombination of the CT state.[18,19] The energy level of the CT state in 1,2-di(1-anthryl)ethane is estimated to be lower than that of the LE state, and hence the CT character is large. In our case, the energy level of the CT state in the *anti*-CzOCz in an MeCN solution is estimated to be 4.2 eV, which is 0.6 eV higher than that of the LE state (details are described in the Supporting Information),[12,35,47,60,61] and hence mixing of the CT state and the LE state would be negligibly small in the *anti*-conformation. This is in good agreement with the solvent-polarity independent monomer emission band. Thus, the conformation of the *int*-CzOCz is probably important to the CT character. Because of the edge-to-face geometry in the *int*-CzOCz, the facial and axial carbazole rings are energetically not equivalent. This is in contrast to the symmetrical geometry in the *anti*- and *syn*-CzOCz. Consequently, as shown in Figure 7b, the molecular orbitals are distributed asymmetrically between two carbazole rings in the *int*-CzOCz, which would be helpful to mix the CT state with the LE state.[62] We therefore conclude that the asymmetrical edge-to-face geometry is a key determinant of the CT character in the *int*-CzOCz in the excited state.

4. Conclusions

We have studied solvent-polarity-induced formation dynamics of the intramolecular excimer in CzOCz by time-resolved spectroscopic methods and computational calculations. In the ground state, the stacking mode of two carbazole rings is the *anti*-conformation, and the isomerization from the *anti*- to *syn*-CzOCz is negligible because of large activation energy. In contrast, in the excited state, the potential barrier for the isomerization is much lower than that in the ground state and becomes lower in polar solutions. The rate-limiting process of the excimer formation is the *anti–int* isomerization, and hence the potential barrier for the isomerization E_{iso} corresponds to the activation energy for the *anti–int* isomerization. Owing to the favorable orbital interaction between the two carbazole rings, the *int*-CzOCz becomes more stable compared to the *anti*-CzOCz in the excited state. This stabilization leads to the decrease in the potential barrier in the excited state. The *int*-CzOCz in polar solutions is more stable because of the CT character in the excited state, resulting in efficient *anti–int* isomerization in polar solutions. We therefore conclude that the efficient excimer formation in polar solvents is attributed to the CT character of the *int*-CzOCz in the excited state. Because of the edge-to-face geometry in the *int*-CzOCz, the facial and axial carbazole rings are energetically not equivalent. Consequently, the molecular orbitals are distributed asymmetrically between two carbazole rings in *int*-CzOCz, which would be helpful to mix the CT state to the LE state. We therefore conclude that the asymmetrical edge-to-face geometry is a key determinant of the CT character in the *int*-CzOCz in the excited state.

5. Experimental Section

Materials. Dioxa[3.3](3,6)carbazolophane (CzOCz) was synthesized by the cyclization reaction between 3,6-bis(hydroxymethyl)carbazole and 3,6-bis(bromomethyl)carbazole, and was purified by alumina chromatography and recrystallization. As a reference, 3,6-bis(methoxymethyl)carbazole (CzOMe) was also prepared. Details of the synthesis have been described elsewhere.[45] Solvents used in

this study were acetonitrile (MeCN, Wako, spectroscopic grade), *N*,*N*-dimethyl formamide (DMF, Nacalai Tesque, spectroscopic grade), and tetrahydrofuran (THF, Wako, spectroscopic grade). These solvents were used without further purification.

Measurements. Absorption and photoluminescence spectra were measured at room temperature in a 1-cm quartz cell with a UV–visible spectrophotometer (Hitachi, U-3500) and a fluorescence spectrophotometer (Hitachi, F-4500) equipped with a red-sensitive photomultiplier (Hamamatsu, R928F), respectively. Photoluminescence decay was measured by the time-correlated single-photon-counting (TCSPC) method (Horiba Jobin Yvon, FluoroCube). The excitation wavelength was 296 nm. The total instrument response function is an fwhm of ca. 800 ps. Transient absorption data were collected with a pump and probe femtosecond transient spectroscopy system. This system consists of a transient absorption spectrometer (Ultrafast Systems, Helios) and a regenerative amplified Ti:sapphire laser (Spectra-Physics, Hurricane). The amplified Ti:sapphire laser provided 800 nm fundamental pulses at a repetition rate of 1 kHz with a power of 0.9 mJ and a pulse width of 100 fs (fwhm), which were split into two optical beams with a beam splitter to generate pump and probe pulses. One fundamental beam was converted into pump pulses at 350 nm with an ultrafast optical parametric amplifier (Spectra-Physics, TOPAS). The other fundamental beam was converted into white light pulses employed as probe pulses in the wavelength region from 400 to 1700 nm. The pump pulses were modulated mechanically with a repetition rate of 500 Hz. The temporal evolution of the probe intensity was recorded with a CMOS linear sensor (Ultrafast Systems, SPEC-VIS) for the visible measurement and with an InGaAs linear diode array sensor (Ultrafast Systems, SPEC-NIR) for the near-IR measurement. The transient absorption spectra and decays were collected over the time range from −5 ps to 3 ns. Typically, 2500 laser shots were averaged at each delay time to obtain a detectable absorbance change as small as ~10^{-4}. In order to cancel out orientation effects on the dynamics, the polarization direction of the linearly polarized probe pulse was set at a magic angle of 54.7 ° with respect to that of the pump pulse. Samples were degassed by Ar bubbling for 30 min. The concentration of carbazole compounds was in the order of 10^{-4} mol L^{-1} for the transient absorption

measurements and 10^{-5} mol L^{-1} for the other measurements. Note that the transient absorption spectra and dynamics were highly reproducible even after the several times measurements. In other words, the laser irradiation had negligible effects on the sample degradation at least under this experimental condition.

Calculations. Gas-phase molecular mechanics calculations of the CzOCz were performed with AMBER10.[52] The CzOCz was assigned to gaff atom types and AM1-BCC charges by using the antechamber module. The molecular structure in the *anti*-, *int*-, and *syn*-conformers was energy-minimized with the sander module. Owing to the reversal symmetry in CzOCz, the dihedral angles in the opposite side, φ_1' and φ_2', can be assumed to be equal to φ_1 and φ_2, respectively. As a function of the dihedral angles φ_1 and φ_2, conformational energy was determined from minimization by applying a very strong harmonic potential around the value of each dihedral angle. All quantum chemical calculations were carried out using Gaussian 09.[53] The ground state optimizations were carried out using the density functional theory (DFT) methods with the CAM-B3LYP functional, which is a long-distance corrected functional, at the 6-31G(d,p) basis set. The excited state optimizations were carried out using time-dependent DFT (TD-DFT) methods with the same level. The effect of solvent environment was simulated using the polarizable continuum model (PCM).[54] The state-specific solvation of vertical transitions (absorption and emission) was accomplished using a procedure described in the g09 manual.[53] Molecular orbitals were visualized by using Molekel 5.4.[63]

Acknowledgment. This work was partly supported by JSPS KAKENHI Grant Number 22550033.

Supporting Information Available: Transient absorption decays of CzOMe and CzOCz, detailed analysis of the kinetics, estimation of energy level of the CT state, asymmetric isomerization pathway, and optimized geometries of CzOCz conformers. This material is available free of charge via the Internet at http://pubs.acs.org.

References

(1) Yanari, S. S.; Bovey, F. A.; Lumry, R. Fluorescence of Styrene Homopolymers and Copolymers. *Nature* **1963**, *200*, 242–244.

(2) Hirayama, F. Intramolecular Excimer Formation. I. Diphenyl and Triphenyl Alkanes. *J. Chem. Phys.* **1965**, *42*, 3163–3171.

(3) Chandross, E. A.; Dempster, C. J. Intramolecular Excimer Formation and Fluorescence Quenching in Dinaphthylalkanes. *J. Am. Chem. Soc.* **1970**, *92*, 3586−3593.

(4) Klöpffer, W. Excimer and Monomer Fluorescence of 1,3-Biscarbazolyl Propane. *Chem. Phys. Lett.* **1969**, *4*, 193−194.

(5) Klöpffer, W. Transfer of Electronic Excitation Energy in Polyvinyl Carbazole. *J. Chem. Phys.* **1969**, *50*, 2337−2343.

(6) Ito, S.; Yamamoto, M.; Nishijima, Y. Kinetic Studies on Intramolecular Excimer Formation in Dinaphthylalkanes. *Bull. Chem. Soc. Jpn.* **1981**, *54*, 35−40.

(7) Ito, S.; Yamamoto, M.; Nishijima, Y. Conformational Analysis of Intramolecular Excimer Formation in Dinaphthylalkanes. *Bull. Chem. Soc. Jpn.* **1982**, *55*, 363−368.

(8) Ito, S.; Takami, K.; Tsujii, Y.; Yamamoto, M. Excimer Formation in Sterically Hindered Poly(9-vinylcarbazole) and Its Dimer Model Compounds. *Macromolecules* **1990**, *23*, 2666−2673.

(9) Birks, J. B. *Photophysics of Aromatic Molecules*; Wiley-Interscience: London, 1970; Chapter 7.

(10) Birks J. B. Excimers. *Rep. Prog. Phys*. **1975**, *38*, 903–974.

(11) Azumi, T.; Armstrong, A. T.; McGlynn, S. P. Energy of Excimer Luminescence. II. Configuration Interaction between Molecular Exciton States and Charge Resonance States. *J. Chem. Phys.* **1964**, *41*, 3839–3852.

(12) Katoh, R.; Sinha, S.; Murata, S.; Tachiya, M. Origin of the Stabilization Energy of Perylene Excimer as Studied by Fluorescence and Near-IR Transient Absorption Spectroscopy. *J. Photochem. Photobiol., A* **2001**, *145*, 23–34.

(13) Amicangelo, J. C. Theoretical Study of the Benzene Excimer Using Time-Dependent Density Functional Theory. *J. Phys. Chem. A* **2005**, *109*, 9174–9182.

(14) Shirai, S.; Iwata, S.; Tani, T.; Inagaki, S. Ab Initio Studies of Aromatic Excimers Using Multiconfiguration Quasi-Degenerate Perturbation Theory. *J. Phys. Chem. A* **2011**, *115*, 7687–7699.

(15) Lim, E. C. Molecular Triplet Excimers. *Acc. Chem. Res.* **1987**, *20*, 8−17.

(16) East, A. L. L.; Lim, E. C. Naphthalene Dimer: Electronic States, Excimers, and Triplet Decay. *J. Chem. Phys.* **2000**, *113*, 8981−8994.

(17) Terazima, M.; Cai, J.; Lim. E. C. Time-Resolved EPR and Optical Studies of Intermoiety Interactions in the Lowest Triplet State of L-Shaped Dimers of Naphthalene: Conformation Dependence of Excitation Exchange Interaction. *J. Phys. Chem. A* **2000**, *104*, 1662−1669.

(18) Mataga, N.; Yao, H.; Okada, T. Picosecond Laser Photolysis Studies on Dimer Model Systems in Relation to Photosynthetic Charge Separation Processes. *Tetrahedron* **1989**, *45*, 4683–4692.

(19) Yao, H.; Okada, T.; Mataga, N. Solvation-Induced Charge Separation in the Excited State of Composite Systems with Identical Halves and Intramolecular Excimer Formation by Recombination. Picosecond Laser Photolysis Studies on 1,2-Dianthrylethanes. *J. Phys. Chem.* **1989**, *93*, 7388–7394.

(20) Mataga, N.; Chosrowjan, H.; Taniguchi, S. Ultrafast Charge Transfer in Excited Electronic States and Investigations into Fundamental Problems of Exciplex Chemistry: Our Early Studies and Recent Developments. *J. Photochem. Photobiol., C* **2005**, *6*, 37–79.

(21) Cram, D. J.; Cram, J. M. Cyclophane Chemistry: Bent and Battered Benzene Rings. *Acc. Chem. Res.* **1971**, *4*, 204–213.

(22) Cram, D. J.; Allinger, N. L.; Steinberg, H. Macro Rings. VII. The Spectral Consequences of Bringing Two Benzene Rings Face to Face. *J. Am. Chem. Soc.* **1954**, *76*, 6132–6141.

(23) Vala, M. T.; Hillier, I. H.; Rice, S. A.; Jortner, J. Theoretical Studies of Transannular Interactions. I. Benzene Excimer Fluorescence and the Singlet States of the Paracyclophanes. *J. Chem. Phys.* **1966**, *44*, 23–35.

(24) Hillier, I. H.; Glass, L.; Rice, S. A. Theoretical Studies of Transannular Interactions. II. The Triplet States of the Paracyclophanes. *J. Chem. Phys.* **1966**, *45*, 3015–3021.

(25) Longworth, J. W.; Bovey, F. A. Conformations and Interactions of Excited States. I. Model Compounds for Polymers. *Biopolymers* **1966**, *4*, 1115–1129.

(26) Froines, J. R.; Hagerman, P. J. Luminescence of Paracyclophanes I. *Syn*- and *Anti*-[2.2] Paracyclophane. *Chem. Phys. Lett.* **1969**, *4*, 135–138.

(27) Yanagidate, M.; Takayama, K.; Takeuchi, M.; Nishimura, J.; Shizuka, H. Molecular Conformation Effects on the Relaxation Processes in the Excited State of Naphthalenophanes. *J. Phys. Chem.* **1993**, *97*, 8881–8888.

(28) Morita, M.; Kishi, T.; Tanaka, M.; Tanaka, J.; Ferguson, J.; Sakata, Y.; Misumi, S.; Hayashi, T.; Mataga, N. Electronic Absorption and Fluorescence Spectra of [2.2]Anthracenophanes. *Bull. Chem. Soc. Jpn.* **1978**, *51*, 3449–3457.

(29) Nakamura, Y.; Tsuihiji, T.; Mita, T.; Minowa, T.; Tobita, S.; Shizuka, H.; Nishimura, J. Synthesis, Structure, and Electronic Properties of *syn*-[2.2]Phenanthrenophanes: First Observation of Their Excimer Fluorescence at High Temperature. *J. Am. Chem. Soc.* **1996**, *118*, 1006–1012.

(30) Nakamura, Y.; Kaneko, M.; Yamanaka, N.; Tani, K.; Nishimura, J. Synthesis and Photophysical Properties of *syn*- and *anti*-[2.*n*](3,9)Carbazolophanes. *Tetrahedron Lett.* **1999**, *40*, 4693–4696.

(31) Tani, K.; Tohda, Y.; Takemura, H.; Ohkita, H.; Ito, S.; Yamamoto, M. Shnthesis and Photophysical Properties of [3.3](3,9)carbazolophanes. *Chem. Commun.* **2001**, 1914–1915.

(32) Nakamura, Y.; Kaneko, M.; Tani, K.; Shinmyozu, T.; Nishimura, J. Synthesis and Properties of Triply-Bridged *syn*-Carbazolophanes. *J. Org. Chem.* **2002**, *67*, 8706–8709.

(33) Ohkita, H.; Ito, S.; Yamamoto, M.; Tohda, Y.; Tani, K. Intramolecular Excimer Emission of *syn*- and *anti*-[3.3](3,9)Carbazolophanes in Solutions. *J. Phys. Chem. A* **2002**, *106*, 2140–2145.

(34) Benten, H.; Ohkita, H.; Ito, S.; Yamamoto, M.; Sakumoto, N.; Hori, K.; Tohda, Y.; Tani, K.; Nakamura, Y.; Nishimura, J. Intramolecular Excimer Emission of Triply Bridged [3.3.*n*](3,6,9)Carbazolophanes. *J. Phys. Chem. B* **2005**, *109*, 19681–19687.

(35) Benten, H.; Guo, J.; Ohkita, H.; Ito, S.; Yamamoto, M.; Sakumoto, N.; Hori, K.; Tohda, Y.; Tani, K. Intramolecular Singlet and Triplet Excimers of Triply Bridged [3.3.*n*](3,6,9)Carbazolophanes. *J. Phys. Chem. B* **2007**, *111*, 10905–10914.

(36) Tani, K.; Sakumoto, N.; Kubono, K.; Hori, K.; Tohda, Y.; Benten, H.; Ohkita, H.; Ito, S.; Yamamoto, M. Synthesis and Photophysical Properties of Tris-bridged [3.3.*n*](3,6,9)Carbazolphanes. *Chem. Lett.* **2009**, *38*, 140–141.

(37) Griffin Jr., R. W.; Coburn, R. A. [3.2]Metacyclophanes. Conformational Studies. *J. Am. Chem. Soc.* **1967**, *89*, 4638–4641.

(38) Sorimachi, K.; Morita, T.; Shizuka, H. Photocyclization of [2.2]Methcyclophane at 2537 Å. *Bull. Chem. Soc. Jpn.* **1974**, *47*, 987–990.

(39) Shizuka, H.; Ogiwara, T.; Morita, T. Weak Fluorescence from [2.2]Metacyclophane. *Bull. Chem. Soc. Jpn.* **1975**, *48*, 3385–3386.

(40) Hayashi, T.; Mataga, N.; Sakata, Y.; Misumi, S. Effects of Solvent Polarity on the Fluorescence Spectrum of [2.2](1,3)Pyrenophane. *Chem. Phys. Lett.* **1976**, *41*, 325–328.

(41) Hayashi, T.; Mataga, N.; Umemoto, T.; Sakata, Y.; Misumi, S. Solvent-Induced Polarization Phenomena in the Excited State of Composite Systems with Identical Halves. 2. Effects of Solvent Polarity upon the Fluorescence of [2.2](1,3)Pyrenophane. *J. Phys. Chem.* **1977**, *81*, 424–429.

(42) Fujise, Y.; Nakasato, Y.; Ito, S. Syn-5,13-Dimethyl[2.2]Metacyclophane. Synthesis, Spectra and Thermal Stability. *Tetrahedron Lett.* **1986**, *27*, 2907–2908.

(43) Mitchell, R. H.; Vinod, T. K.; Bushnell, G. W. *syn*-[2.2]Metacyclophane: Isolation, NMR Properties, and Facile Isomerization to *anti*-[2.2]Metacyclophane. A Synthesis Involving Bridge Reactions of Chromium Tricarbonyl Complexed Dithiametacyclophanes. *J. Am. Chem. Soc.* **1990**, *112*, 3487–3497.

(44) Ito, S.; Nakasato, Y.; Hioki, H.; Nagaku, M.; Kan, Y.; Fukazawa, Y. Benzene Ring Flipping in *syn*[2.2]Metacyclophanes: Effect of Substituents. *Tetrahedron Lett.* **1993**, *34*, 3789–3792.

(45) Tani, K.; Tohda, Y.; Hisada, K.; Yamamoto, M. Synthesis and Properties of Dioxa[3.3](3,6)carbazolophane. *Chem. Lett.* **1996**, 145–146.

(46) Johnson, G. E. A Spectroscopic Study of Carbazole by Photoselection. *J. Phys. Chem.* **1974**, *78*, 1512–1521.

(47) Johnson, G. E. Emission Properties of Vinylcarbazole Polymers. *J. Chem. Phys.* **1975**, *62*, 4697−4709.

(48) Bonesi, S. M.; Erra-Balsells, R. Electronic Spectroscopy of Carbazole and N- and C-Substituted Carbazoles in Homogeneous Media and in Solid Matrix. *J. Lumin.* **2001**, *93*, 51–74.

(49) Loughnane, B. J.; Scodinu, A.; Farrer, R. A.; Fourkas, J. T.; Mohanty, U. Exponential Intermolecular Dynamics in Optical Kerr Effect Spectroscopy of Small-Molecule Liquids. *J. Chem. Phys.* **1999**, *111*, 2686–2694.

(50) Szwarc, M. *Carbanions Living Polymers and Electron Transfer Processes*; Interscience, N.Y., 1968

(51) Masuhara, H.; Tamai, N.; Mataga, N.; De Schryver, F. C.; Vandendriessche, J.; Boens, N. Excimer Formation in Poly(N-vinylcarbazole) and Its Model Compounds as Revealed by Picosecond Time-Resolved Absorption Spectroscopy. *Chem. Phys. Lett.* **1983**, *95*, 471–475.

(52) AMBER10, Case, D. A.; Darden, T. A.; Cheatham, III, T. E.; Simmerling, C. L.; Wang, J.; Duke, R. E.; Luo, R.; Crowley, M.; Walker, R. C.; Zhang, W. et al. AMBER 10, University of California, San Francisco, 2008.

(53) Gaussian 09, Revision C.01, Frisch, M. J.; Trucks, G. W.; Schlegel, H. B.; Scuseria, G. E.; Robb, M. A.; Cheeseman, J. R.; Scalmani, G.; Barone, V.; Mennucci, B.; Petersson, G. A. et al. Gaussian, Inc., Wallingford CT, 2009.

(54) Tomasi, J.; Mennucci, B.; Cammi, R. Quantum Mechanical Continuum Solvation Models. *Chem. Rev.* **2005**, *105*, 2999–3093.

(55) Huenerbein, R.; Grimme, S. Time-dependent Density Functional Study of Excimers and Exciplexes of Organic Molecules. *Chem. Phys.* **2008**, *343*, 362–371.

(56) Nakashima, N.; Murakawa, M.; Mataga, N. Picosecond Flash Spectroscopy of Solvent-Induced Intramolecular Electron Transfer in the Excited 9,9'-Bianthryl. *Bull. Chem. Soc. Jpn.* **1976**, *49*, 854–858.

(57) Mataga, N.; Yao, H.; Okada, T.; Rettig, W. Charge-Transfer Rates in Symmetric and Symmetry-Disturbed Derivatives of 9,9'-Bianthryl. *J. Phys. Chem.* **1989**, *93*, 3383–3386.

(58) Mataga, N.; Nishikawa, S.; Okada, T. Torsional Relaxations from Perpendicular to Tilted Configurations in the Intramolecular Charge Transfer of Excited 9,9'-Bianthryl as Studied by Femtosecond-Picosecond Time-Resolved Absorption Spectral Measurements in Solution. *Chem. Phys. Lett.* **1996**, *257*, 327–332.

(59) Grabowski, Z. R.; Rotkiewicz, K.; Rettig, W. Structural Changes Accompanying Intramolecular Electron Transfer: Focus on Twisted Intramolecular Charge-Transfer States and Structures. *Chem. Rev.* **2003**, *103*, 3899–4031.

(60) Sharp, J. H. Charge-Transfer Complexes of N-Isopropylcarbazole. *J. Phys. Chem.* **1966**, *70*, 584–586.

(61) Katoh, R.; Katoh, E.; Nakashima, N; Yuuki, M.; Kotani, M. Near-IR Absorption Spectrum of Aromatic Excimers. *J. Phys. Chem. A* **1997**, *101*, 7725–7728.

(62) Lee, E. C.; Hong, B. H.; Lee, J. Y.; Kim, J. C.; Kim, D.; Kim, Y.; Tarakeshwar, P.; Kim, K. S. Substituent Effects on the Edge-to-Face Aromatic Interactions. *J. Am. Chem. Soc.* **2005**, *127*, 4530–4537.

(63) Varetto, U.; MOLEKEL 5.4.; *Swiss National Supercomputing Centre: Lugano, Switzerland.*

FIGURE CAPTIONS

Figure 1. Chemical structures of dioxa[3.3](3,6)carbazolophane (CzOCz) in *syn*- and *anti*-conformation and 3,6-bis(methoxymethyl)-*N*-ethylcarbazole (CzOMe) as a reference.

Figure 2. (a) Absorption spectra of CzOCz (black solid), and CzOMe (gray solid) in an MeCN solution at room temperature. (b) Fluorescence spectra of CzOCz (black lines) and CzOMe (gray line) in an MeCN solution at room temperature. The fluorescence spectra of CzOCz were measured after Ar (black solid) and O_2 (black broken) bubbling. The red spectrum was obtained by subtracting black broken from black solid. (c) Fluorescence spectra of CzOCz in MeCN (black solid), DMF (black broken), and THF (gray solid) solutions at room temperature.

Figure 3. (a) Time-resolved emission spectra of CzOCz in an MeCN solution at room temperature measured at 0.5, 3, 5, 7.5, 10, and 20 ns after the laser excitation. (b) Fluorescence decay curves of CzOCz and CzOMe in an MeCN solution at room temperature: excimer emission of CzOCz (red circles), monomer emission of CzOCz (green triangles), and monomer emission of CzOMe (blue squares). The gray broken line represents an instrument response function. The solid lines represent fitting curves with two (red) and one (green and blue) exponential functions, respectively.

Figure 4. Arrhenius plots of the apparent excimer formation rate constant k_{ex} of CzOCz in an MeCN solution against the temperature from 273 to 323 K. The apparent excimer formation rate constant k_{ex} was estimated as $k_{ex} = 1/\tau_{mono} - 1/\tau_f^0$. The solid line represents the fitting curve with the Arrhenius equation: $\ln k_{ex} = \ln A - E_a/RT$. From the best fitting result, the pre-exponential factor A was estimated to be 8.6×10^{10} s^{-1} for all the solvents employed. The apparent activation energy E_a was estimated to be 12.3 kJ mol^{-1} for an MeCN solution and 16.1 kJ mol^{-1} for a THF solution.

Figure 5. Transient absorption spectra of (a–c) CzOCz and (d) CzOMe solutions measured at (purple) 1, (blue) 10, (green) 100, (yellow) 500, (orange) 1000, and (red) 3000 ps after the laser excitation at 350 nm (~30 μJ cm^{-2}). Solvents were (a) MeCN, (b, d) DMF, and (c) THF.

Figure 6. (a) Definition of the dihedral angles φ_1 and φ_2. The dihedral angles in the opposite side, φ_1' and φ_2', are assumed to be the same as φ_1 and φ_2, respectively. (b) Potential energy surface of CzOCz in the ground state as a function of the dihedral angles φ_1 and φ_2 calculated by using generalized AMBER force field (gaff). Three local potential minima, *anti*-, *int*-, and *syn*-conformers, are marked as ●. (c) Potential energy curves along the solid lines in the panel (b).

Figure 7. (a) Optimized structures of CzOCz isomers in the ground (the first and second rows), and excited state (the third row) calculated with the (TD-)DFT/CAM-B3LYP level at the 6-31G(d,p) basis set. (b) Relevant molecular orbitals HOMO−1, HOMO, LUMO, and LUMO+1 in CzOCz conformers calculated with the TD-DFT/CAM-B3LYP level at the 6-31G(d,p) basis set.

Figure 8. Mulliken charge difference between two carbazole rings in the excited state: (a) *anti*-CzOCz, (b) *int*-CzOCz, and (c) *syn*-CzOCz. The red and blue regions represent positively and negatively charged units than that of corresponding units in another carbazole ring, respectively.

SCHEME TITLES

Scheme 1. Schematic Energy Diagram of LE and CT bands in the Excimer State.

Scheme 2. Kinetic Scheme for the Intramolecular Excimer Formation.

Scheme 3. Schematic Illustration of Potential Curve for Intramolecular Excimer Formation.

TABLES

Table 1. ^{1}H NMR Chemical Shifts of Aromatic Protons in CzOCz and CzOMe.

Table 2. Fitting Parameters for Fluorescence Decay and Apparent Excimer Formation Rate Constants.

Table 3. Vertical Transition Energies and Energy Difference Calculated.

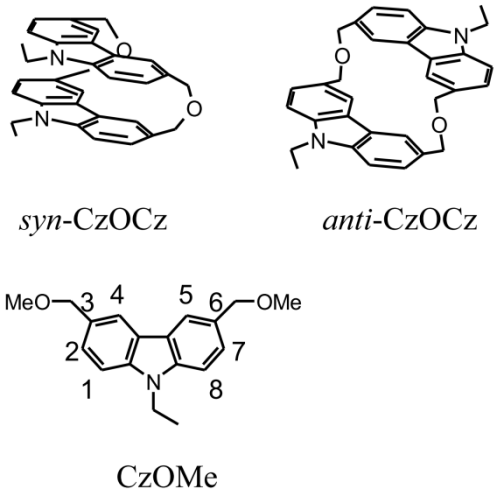

Figure 1

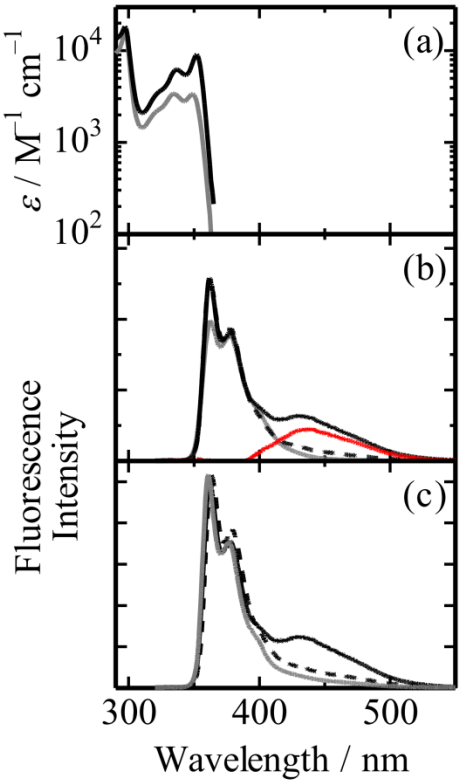

Figure 2

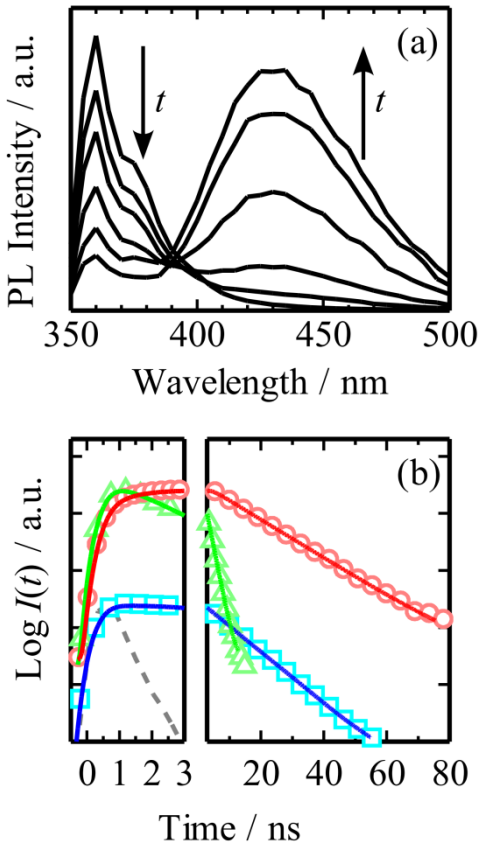

Figure 3

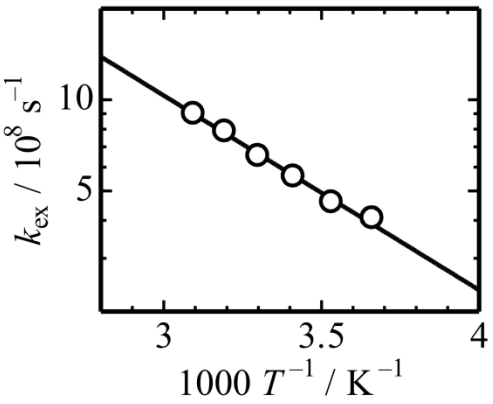

Figure 4

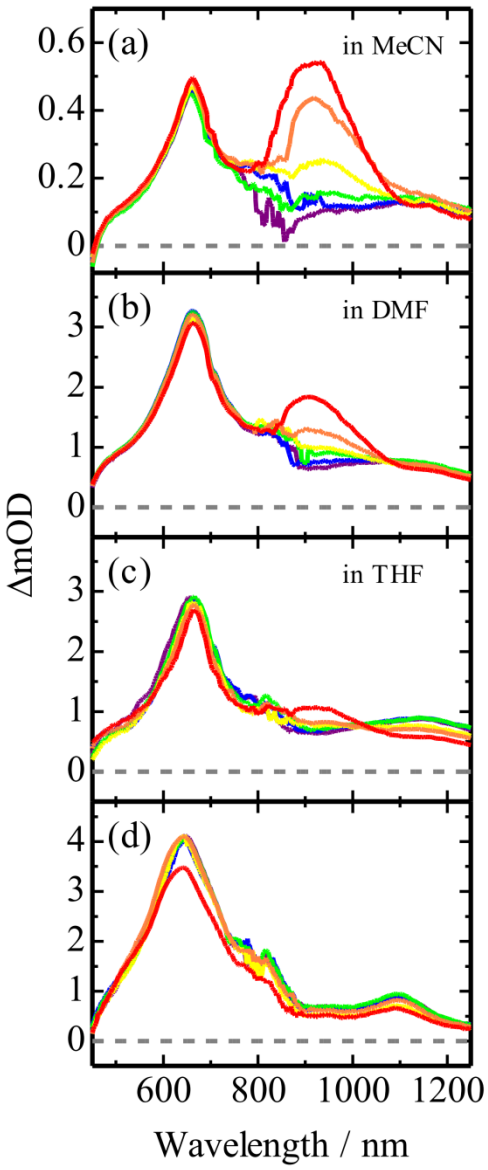

Figure 5

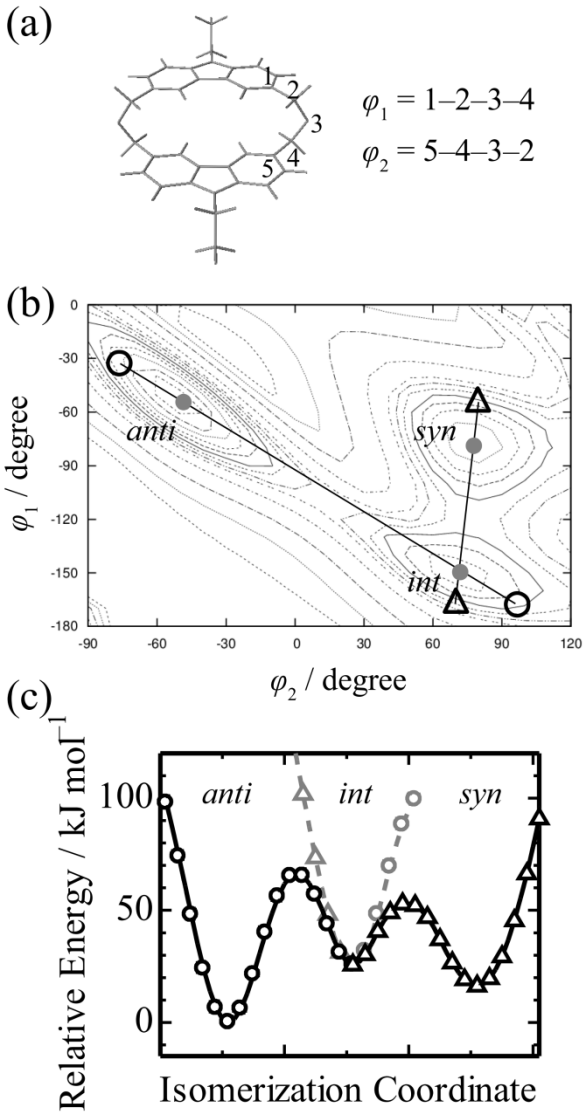

Figure 6

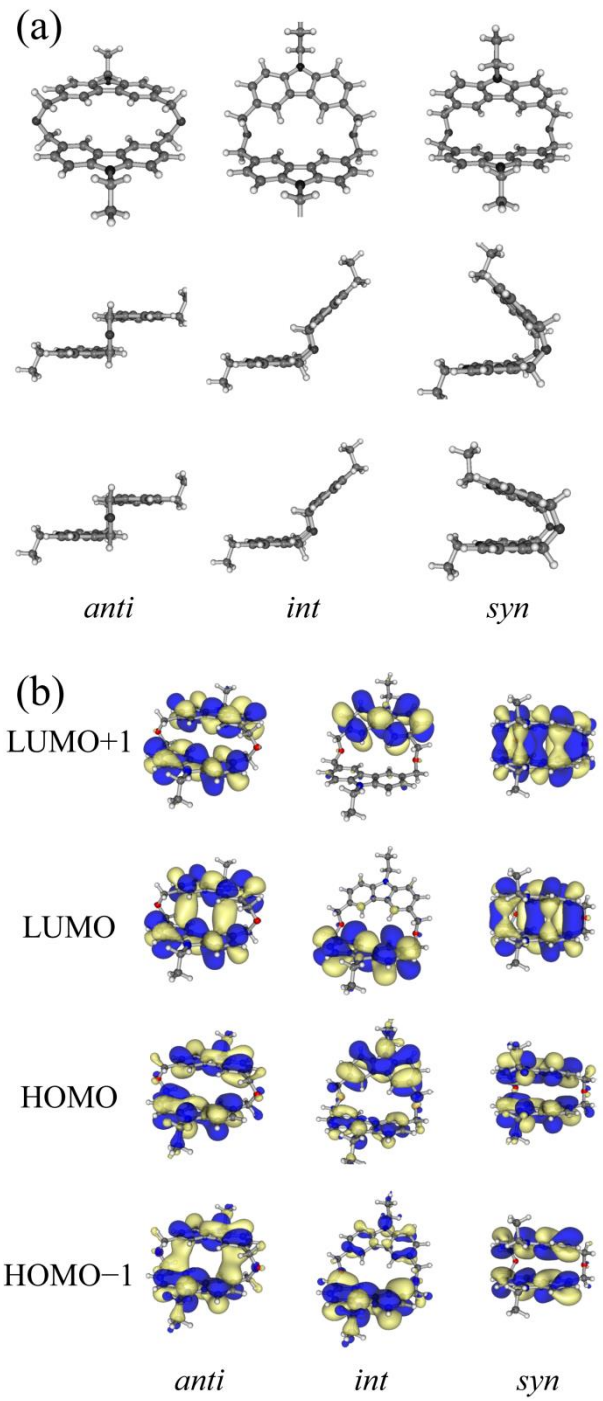

Figure 7

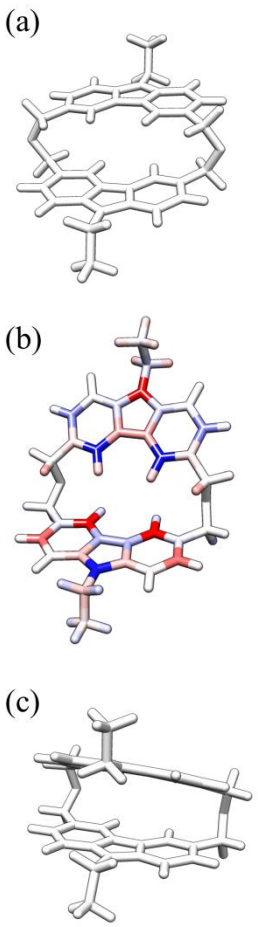

Figure 8

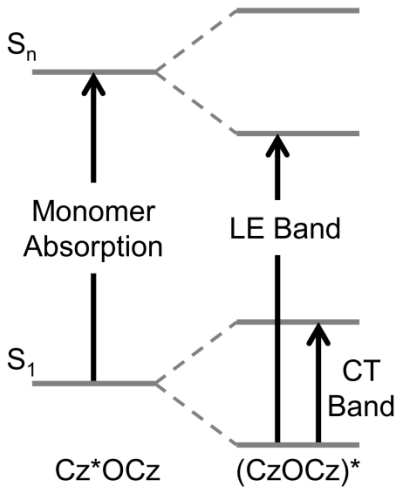

The LE band is a transition from the lowest excimer state to a higher state, and has almost the same spectral position as the monomer S_1–S_n transition. The CT band is a transition from the lowest excimer state to the second lowest state which has a CT character. The CT band is observed regardless of the strength of the CT character in the excimer state, but the spectral position of the CT band is strongly dependent on the molecular structure.

Scheme 1

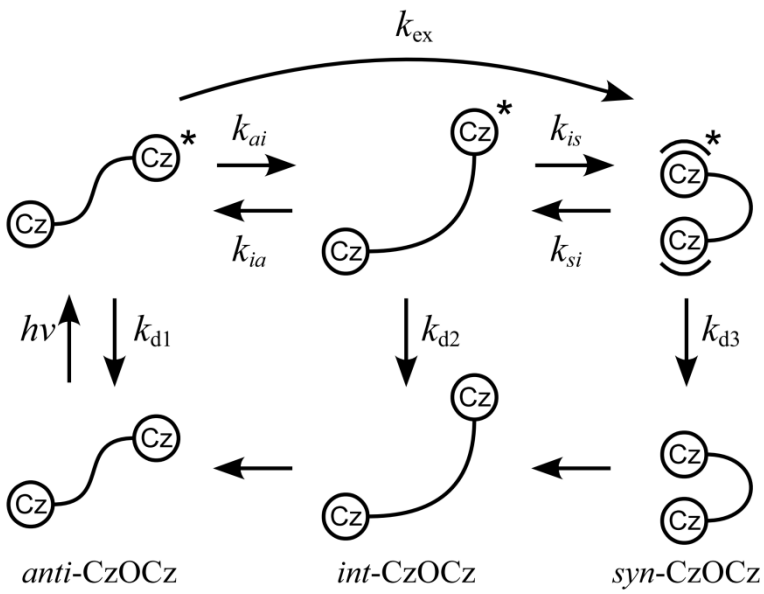

The rate constants k_{d1}, k_{d2}, and k_{d3} are due to radiative and non-radiative monomolecular deactivations of *anti*-, *int*-, and *syn*-CzOCz, respectively. The rate constants k_{ai}, k_{is}, k_{ia}, and k_{si} are the isomerization rate constants in the excited state. The rate constant k_{ex} represents the apparent excimer formation rate of the intramolecular excimer.

Scheme 2

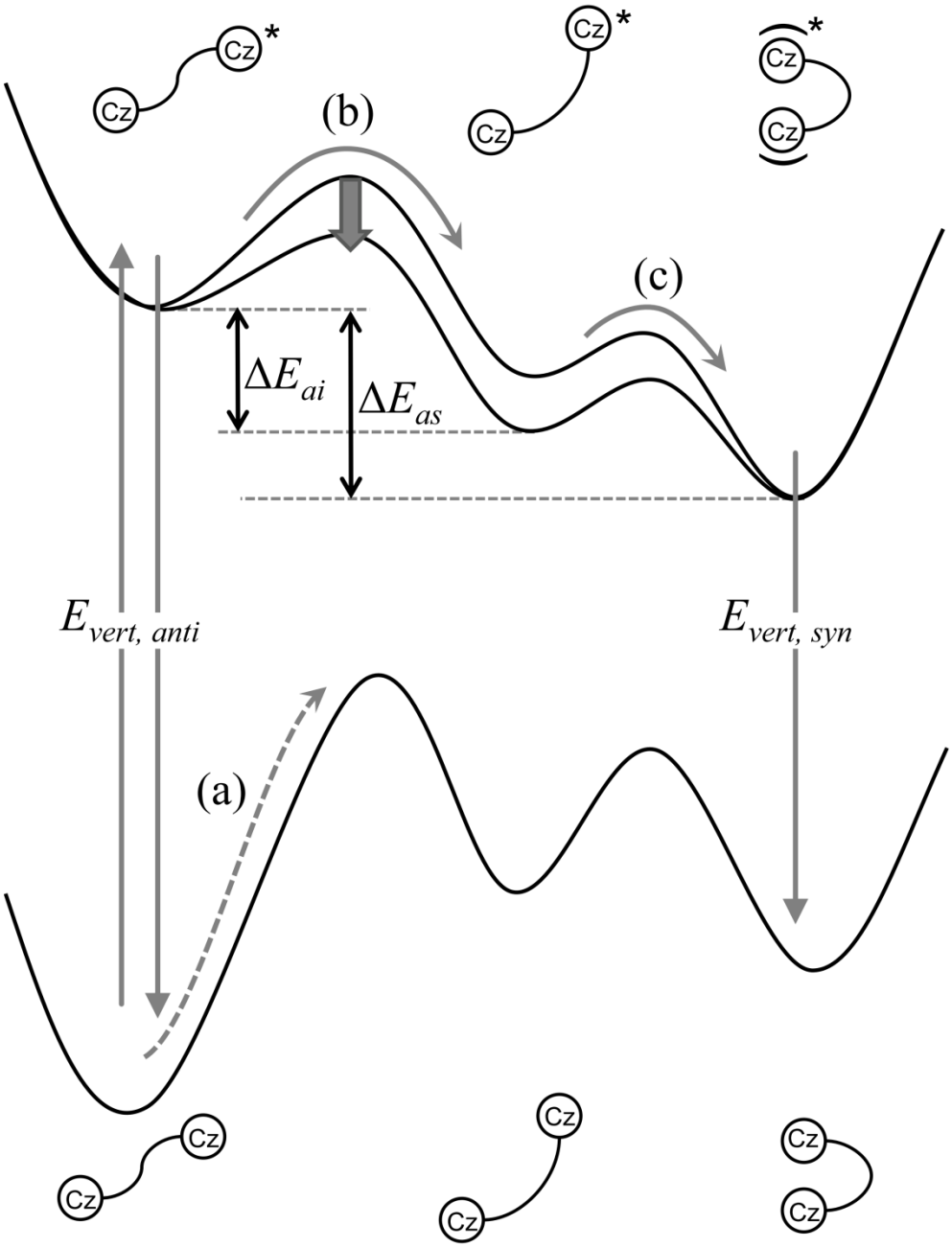

The *anti–int* isomerization is negligible in the ground state because of high potential barrier (a). In contrast, the potential barrier in the excited state is much lower than that in the ground state, and hence the isomerization easily undergoes (b). Because the potential barrier becomes lower in polar solutions, the *int*-conformer is formed more efficiently in polar solutions. Once, the *int*-conformer is formed, the subsequent isomerization from the *int*- to *syn*-conformer undergoes immediately because of lower potential barrier (c).

Scheme 3

Table 1

	H1/H8	H2/H7	H4/H5
CzOCz	7.48	7.64	8.15
CzOMe	7.41	7.58	8.10

Table 2

	360 nm (decay, ns)	450 nm (rise, ns)	450 nm (decay, ns)	k_{ex} [a] (10^8 s^{-1})
in MeCN	1.6	1.5	12.9	5.6
in DMF	3.1	3.1	12.9	2.1
in THF	4.4	4.2	12.6	1.3
CzOMe	9.5	—	—	—

[a] The apparent excimer formation rate constant k_{ex} was estimated as $k_{ex} = 1/\tau_{mono} - 1/\tau_f^0$.

Table 3

	$E_{vert,\ anti}$ (kJ mol^{-1})	$E_{vert,\ syn}$ (kJ mol^{-1})	ΔE_{ai} (kJ mol^{-1})	ΔE_{as} (kJ mol^{-1})
Vaccum	415 (4.30)	345 (3.57)	−1.8	−15.1
in MeCN	411 (4.26)	348 (3.61)	−8.8	−16.2
in THF	412 (4.27)	348 (3.60)	−6.7	−15.0

The vertical transition energies in parenthesis are in eV scale.

Table of Contents graphic

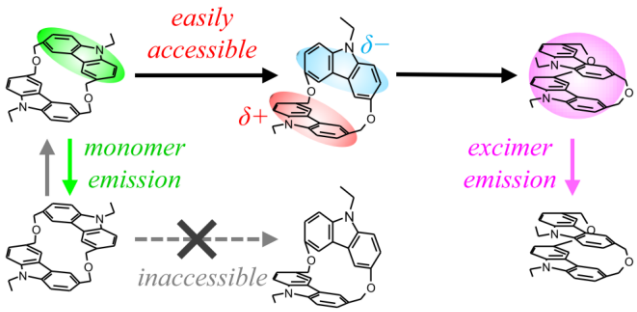

Dioxa[3.3](3,6)carbazolophane